Environ. Sci. Technol. **2003**, *37,* 3828−3837

Particle Growth by Acid-Catalyzed Heterogeneous Reactions of Organic Carbonyls on Preexisting Aerosols

MYOSEON JANG,* BRIAN CARROLL, BHARADWAJ CHANDRAMOULI, AND RICHARD M. KAMENS

Department of Environmental Sciences and Engineering, CB 7431, Rosenau Hall, The University of North Carolina at Chapel Hill, Chapel Hill, North Carolina 27599

Aerosol growth by the heterogeneous reactions of different aliphatic and α,β-unsaturated carbonyls in the presence/absence of acidified seed aerosols was studied in a 2 m long flow reactor (2.5 cm i.d.) and a 0.5-m^3 Teflon film bag under darkness. For the flow reactor experiments, 2,4-hexadienal, 5-methyl-3-hexen-2-one, 2-cyclohexenone, 3-methyl-2-cyclopentenone, 3-methyl-2-cyclohexenone, and octanal were studied. The carbonyls were selected based on their reactivity for acid-catalyzed reactions, their proton affinity, and their similarity to the ring-opening products from the atmospheric oxidation of aromatics. To facilitate acid-catalyzed heterogeneous hemiacetal/acetal formation, glycerol was injected along with inorganic seed aerosols into the flow reactor system. Carbonyl heterogeneous reactions were accelerated in the presence of acid catalysts (H_2SO_4), leading to higher aerosol yields than in their absence. Aldehydes were more reactive than ketones for acid-catalyzed reactions. The conjugated functionality also resulted in higher organic aerosol yields than saturated aliphatic carbonyls because conjugation with the olefinic bond increases the basicity of the carbonyl leading to increased stability of the protonated carbonyl. Aerosol population was measured from a series of sampling ports along the length of the flow reactor using a scanning mobility particle sizer. Fourier transform infrared spectrometry of either an impacted liquid aerosol layer or direct reaction of carbonyls as a thin liquid layer on a zinc selenide FTIR disk was employed to demonstrate the direct transformation of chemical functional groups via the acid-catalyzed reactions. These results strongly indicate that atmospheric multifunctional organic carbonyls, which are created by atmospheric photooxidation reactions, can contribute significantly to secondary organic aerosol formation through acid-catalyzed heterogeneous reactions. Exploratory studies in 25- and 190-m^3 outdoor chambers were also implemented to demonstrate the formation of high molecular weight organic structures. The reaction of ozone with α-pinene to generate secondary organic aerosols (SOAs) was performed in the presence of background aerosol consisting of a mixture of wood soot and diesel soot. Results strongly suggest that indigenous sulfuric acid associated with the combustion of fossil fuels (e.g., diesel soot) can initiate acid-catalyzed heterogeneous reactions of SOAs on the particle phase.

Introduction

Gas-phase reactions of volatile organic compounds (VOCs) associated with photochemical oxidant cycles have been of great interest in predicting O_3 concentrations and, more recently, secondary organic aerosol (SOA) formation. SOAs are a major contributor to fine particulate matter ($PM_{2.5}$) and have potentially negative health effects. In particular, it is believed that the potency of a mixture of environmental chemicals in the particle phase, such as organic/inorganic multicomponents, may be greater than its constitutive parts (*1*). At the regional scale, SOA formation may contribute to the formation of visibility-reducing haze (*2*, *3*). SOA can affect the earth's radiative balance (*4*, *5*) directly by altering the scattering properties of the atmosphere and indirectly by changing cloud properties.

Biogenic terpenes from terrestrial vegetation (*6*−*17*) and aromatics from anthropogenic sources (*18*−*20*) are known to be SOA precursors. The gas-phase photooxidation reactions of these VOCs generate large amounts of multifunctional organic carbonyls (*14*−*17*, *19*, *20*), which are potentially toxic (*21*−*24*). Carbonyls also serve as an important source of organic peroxy and peroxyacyl nitrates via gas-phase photooxidation reactions in the presence of NO_x (*15*). However, little is known about the heterogeneous chemistry of atmospheric carbonyls in the aerosol phase, their overall importance with respect to SOA formation, or how they change as particles age. Our previous studies (*1*, *25*) strongly suggest that carbonyl species can be further transformed via acid-catalyzed heterogeneous reactions between the gas phase and atmospheric particulate matter. The outcome is an increase in SOA mass because the new heterogeneous aerosol reaction products have relatively low vapor pressures and the reaction leads to additional partitioning of the parent compounds from the gas to the particle phase.

Principal candidates for atmospheric acid catalysts are sulfuric acid (H_2SO_4) and nitric acid (HNO_3), which are produced through the oxidation of SO_2 and NO_x emitted from fossil fuel combustion (*26*−*28*). Unlike HNO_3, the H_2SO_4 exists dominantly in the atmospheric particle phase since H_2SO_4 is much less volatile under ambient atmospheric conditions than HNO_3. Most work focusing on inorganic nitrate and sulfate components neglect the organic aerosol fraction. Recently, it has been reported that the reduction of SOA yields from the α-pinene with ozone depends on electrolytes, which differently influence the dissolution of organic products in water associated with seed aerosols (*29*). Up to this point, studies of SOA formation chemistry and kinetics, however, do not consider inorganic components such as atmospheric inorganic acids associated with inorganic salts.

In this study, particle growth by accommodation of different carbonyls onto preexisting seed aerosols was undertaken in a flow reactor and in a 0.5-m^3 Teflon film bag both with and without H_2SO_4 as an acid seed particle catalyst. The objectives of this study were to (i) examine heterogeneous acid-catalyzed reactions of different carbonyls (e.g., aliphatic vs α,β-conjugated aldehydes), (ii) observe the formation of high molecular weight structures in the particle phase via acid-catalyzed heterogeneous reactions, and (iii) evaluate the importance of preexisting indigenous acids in combustion particles for heterogeneous reactions of SOA carbonyls.

* Corresponding author e-mail: mjang@email.unc.edu; telephone: (919)966-3861; fax: (919)966-7911.

10.1021/es021005u CCC: $25.00
Published on Web 07/29/2003

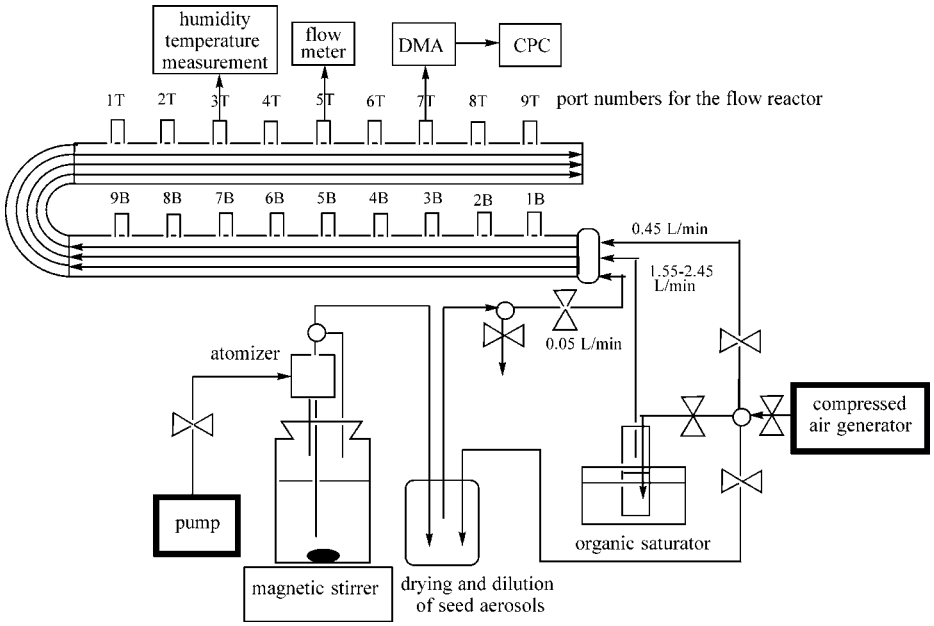

FIGURE 1. Flow reactor illustration (not to scale).

TABLE 1. Experimental Conditions and Organic Aerosol Yields for Heterogeneous Reactions of Diverse Carbonyls in the Flow Reactor with/without an Acid Catalyst: $(NH_4)_2SO_4$ or $(NH_4)_2SO_4-H_2SO_4$ Seed Aerosols Injection with Gas-Phase Carbonyls

date	catalyst	carbonyls	% RH	concn[a] (μL/m^3)	port[b]	seed (nm^3/cm^3)	particles (nm^3/cm^3)	Y	port[b]	seed (nm^3/cm^3)	particles (nm^3/cm^3)	Y
3/21/02	H_2SO_4	2,4-cyclohexadienal	18	6749	7B	1.56E+10	2.60E+10	5.39	7T	1.64E+10	3.52E+10	9.26
3/22/02	non	2,4- cyclohexadienal	20	6798	7B	1.12E+10	1.31E+10	1.53	7T	1.06E+10	1.26E+10	1.47
3/30/02	H_2SO_4	5-methyl-3-hexen-2-one	13	10718	7B	1.18E+10	1.36E+10	2.11	7T	1.23E+10	1.67E+10	4.95
4/19/02	non	5-methyl-3-hexen-2-one	19	10636	7B	1.25E+10	1.30E+10	0.38	7T	1.13E+10	1.04E+10	−0.11
4/5/02	H_2SO_4	2-cyclohexenal	14	6774	7B	3.17E+10	3.76E+10	0.99	7T	3.17E+10	3.68E+10	0.86
4/25/02	non	2-cyclohexenal	17	7229	7B	7.90E+09	8.50E+09	0.38	7T	7.90E+09	8.99E+09	0.69
4/12/02	H_2SO_4	3-methyl-2-cyclopentenone	16	1695	7B	2.67E+10	2.62E+10	−0.47	7T	1.97E+10	2.32E+10	4.45
4/27/02	non	3-methyl-2-cyclopentenone	16	1698	7B	1.18E+10	1.22E+10	0.79	7T	1.02E+10	1.05E+10	0.72
4/6/02	H_2SO_4	3-methyl-2-cyclohexenone	16	893	7B	3.49E+10	3.43E+10	−0.32	7T	2.72E+10	3.12E+10	2.74
4/26/02	non	3-methyl-2-cyclohexenone	14	889	7B	8.09E+09	8.05E+09	−0.09	7T	6.39E+09	6.93E+09	1.58
4/18/02	H_2SO_4	octanal	16	1175	7B	1.41E+10	1.61E+10	2.38	7T	1.41E+10	1.76E+10	4.08
5/13/02	non	octanal	19	1334	7B	1.12E+10	1.15E+10	0.37	7T	1.12E+10	1.25E+10	1.62

[a] The units of gas concentrations injected to the flow reactor are μL (liquid volume of an organic compound)/m^3 (air volume). It is assumed that the densities of a organic compound, seed aerosols, and organic aerosols are same as one (g/mL). [b] See Figure 1 for the port number.

Experimental Section

Flow Reactor. The flow reactor was used to qualitatively examine the acid catalyst effects on organic aerosol formation from the different carbonyl species. The experimental flow reactor used in this study has been reported previously (*30*). Briefly, airstreams containing gas and particles were mixed at the inlet of a glass tube flow reactor (2.0 m length × 2.5 cm i.d.) using multi-angular Teflon inlet plates (*1*, *25*, *29*) to accomplish rapid gas−particle mixing. The flow then immediately entered the main body of the reactor at flow rates ranging from 2.05 to 2.95 L/min (Reynolds no. 72−105). Sampling ports were placed every 10 cm along the length of the flow reactor. Dry air from a pure air generator (AADCO 737, Rockville, MD) was used as a bath gas and for chemical injections. Figure 1 shows the experimental layout used in this study and the numbering of the sampling ports in the flow reactor system. The aerosol population sampled at the ports spaced sequentially down the flow reactor was observed in the absence/presence of an acid catalyst. The seed aerosol was generated using a commercially available large-volume nebulizer (TSI model 3076 constant output atomizer, St. Paul, MN) to aspirate aqueous salt solution into the flow reactor. Two different kinds of seed aerosols were generated; non-acidic, from a 3.4×10^{-3} M ammonium sulfate [$(NH_4)_2SO_4$] solution, and acidic, from 1.7×10^{-3} M $(NH_4)_2SO_4$ and 2.5×10^{-3} M H_2SO_4 aqueous solution. Glycerol (9.86×10^{-3} M) was included in the precursor seed aerosol solution to facilitate the formation of hemiactal/hemiketal and acetal/ketal via the reaction of glycerol with carbonyls. Seed aerosols generated from the nebulizer were diluted with dry air (0.5 L/min). The seed aerosol flow to the flow reactor was controlled at a flow of about 0.05 L/min.

Carbonyls were introduced into the gas phase of the reactor by bubbling dry air through an organic saturator at a flow rate of 1.55−2.45 L/min. The air entering the organic saturator was heated to 40 °C. Additional clean air at a flow rate of 0.45 L/min was brought into the inlet of the flow reactor to help mixing at the inlet (Figure 1). The flow reactor temperature during the course of the experiments was 297−298 K, and the relative humidity (RH) was varied from 10 to 15%. Table 1 shows experimental conditions and aerosol yields from the heterogeneous reaction of carbonyls.

Teflon Film Bag Experiments. The heterogeneous reactions of glyoxal were studied in 0.5-m^3 Teflon film bags (2 mil). All the carbonyls, with the exception of glyoxal, were easily vaporized into the bags. Glyoxal injection to the gas-phase atmosphere of the chambers was carried out by volatilizing aqueous glyoxal solution (wt % = 40) in a hot

TABLE 2. Molecular Structure and Physical Properties of Carbonyls Used for This Study

Compounds	structure	MW	pK_{BH-}	[a] p_L^o at 298 K	[c] $\log K_p$	Types of Exp.
2, 4-hexadienal	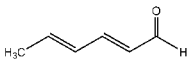	96	-2.4	5.23	-5.71	flow reactor Teflon bag FTIR
3-methyl-2-cyclopentenone	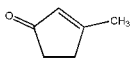	96	-2.82	3.98	5.60	flow reactor Teflon bag FTIR
2-cyclohexenone		96	-3.6	3.46	5.54	flow reactor Teflon bag FTIR
3-methyl-2-cyclohexenone	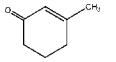	110	-2.83	1.39	5.14	flow reactor Teflon bag FTIR
5-methyl-3-hexen-2-one	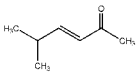	112	-3.8	12.18	-6.08	flow reactor Teflon bag FTIR
octanal	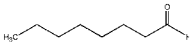	128	< -7	1.34 (0.87) [b]	5.06	flow reactor Teflon bag FTIR
2-hexenal	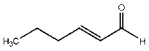			7.90		Teflon bag
mesityl oxide	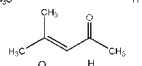			19.94		Teflon bag
glyoxal		58	2.0-3.5	1.56		Teflon bag FTIR
cis-pinonaldehyde	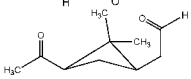	168		0.063		FTIR GC/MS

[a] The vapor pressure (p_L^o) was calculated by (*33, 34*):

$$\ln P^0 = \frac{\Delta S_{vap}(T_b)}{R}\left[(1.8)\left(1 - \frac{T_b}{T}\right) + (0.8)\left(\ln \frac{T_b}{T}\right)\right] \text{(atm)} \quad \text{(A)}$$

where ΔS_{vap} is the entropy of vaporization, R is a gas constant (8.314 J K^{-1} mol^{-1}), T_b is a boiling point (K), and T is an ambient temperature (K) for a given organic compound. ΔS_{vap} of an organic compound was calculated using modified Trouton's method developed by Yalkowsky and co-workers considering parameters related to molecular geometry and association (*35*, *36*). Boiling points (T_b) of organic compounds were calculated by a group contribution method originally developed by Joback and Reid (*37*) with a modified equation and modified group contribution parameters (*38*). [b] Regression method. The Antoine-type equation was used for correlation of vapor pressure as a function of temperature: $\log p_L^o$ (mmHg) $= A + B/T + C \log T + DT + ET^2$ where $A-E$ are regression coefficients for a given compound and T is temperature (K) (*32*). [c] From eq 2. The K_p value was calculated for the carbonyl species used in the flow reactor experiment.

manifold. Glyoxal, however, is readily polymerized at temperatures >150 °C. So on average, only 2 wt % of the total glyoxal injection, calculated from density (1.265 g/mL) and wt % in water solution volatilized into the bag (*25*). Glyoxal in the gas phase of the Teflon bag exists as a mixture of hydrates, monomeric, and oligomeric forms due to the reactive nature of glyoxal. Prior to the addition of organics, acidic seed aerosols, which were made of 0.0034 M $(NH_4)_2SO_4$ and 0.005 M H_2SO_4 aqueous solution, were added to the Teflon bags. The aerosol was generated using a commercially available large volume nebulizer (see Flow Reactor section). The bag temperature was 294−296 K, and the relative humidity was 45−47% during the course of the reactions.

Outdoor Chamber Experiments. The outdoor chamber experiments were conducted in dual 25-m^3 Teflon film chambers at the University of North Carolina at Chapel Hill's outdoor smog chamber facility, located near Pittsboro, NC (June 4, 2002) (*11*−*13*, *17*, *20*). Chamber experiments were conducted under darkness to exclude photochemical effects. To demonstrate particle-phase heterogeneous reactions of SOA products in the presence of real background aerosols, 0.32 ppm of α-pinene was reacted with 0.3 ppm of ozone in the presence of a binary mixture of diesel soot and wood soot. Wood smoke was introduced first into both chambers, denoted as east and west chambers, by burning dry yellow pine in an Arrow catalytic wood stove operated in catalyst bypass mode (*31*). Diesel soot was then injected in both east and west chambers, and ozone was injected to only the east chamber. α-Pinene was then injected into the east chamber. The experimental temperature was 295−300 K, and relative humidity was 46%. The particle mass was collected on 47-mm Teflon-impregnated glass fiber filters (type T60A20, Pallflex Products Corp., Putnam, CT) using a filter−filter−denuder system. The extraction and workup processes have been reported previously (*11*, *31*). Briefly, the filter samples were Soxhlet-extracted for 6 h using dichloromethane, and the denuder samples were rotary-evaporated to 5 mL. Then, both filter and denuder samples were reduced in a volume to 200 μL under a nitrogen stream for the further analyses using a GC/MS.

Materials and Instruments. All compounds except *cis*-pinonaldehyde were purchased from Aldrich (Milwaukee, WI), and are listed in Table 2 along with their calculated vapor pressures (*32*−*38*). The total particle number and size distribution of the aerosols were monitored with a scanning mobility particle sizer (SMPS 3936 TSI, Shoreview, MN) linked to a TSI condensation nuclei counter (3025A, TSI). The SMPS measured particle size data over a size range of 13.8−697 nm. The aerosol sampling flow was operated at 0.3 L/min with a sheath air flow rate of 3 L/min. The scanning time and the residence time (t_f) for the aerosol through the internal plumbing column of the SMPS classifier were 180 and 7.3 s, respectively. Possible uncertainties in measuring aerosol populations are (i) particle off-gassing by the dilution sheath air in the SMPS and (ii) loss of gas-phase organics by heterogeneous reactions on the walls. The estimated particle deposition on the flow reactor tube at sampling port 7B and 7T is less than 1%, when the averaged particle geometric

mean diameter is 50 nm and the total air flow in the reactor tube is 2.3 L/min.

The analysis of functional group transformations in the liquid phase was performed using a Fourier transform infrared spectroscopy (FTIR) (Nicollet Magma 560, Madison, WI) with a deuterated triglycine sulfate (DTGS) detector. The individual carbonyls used in the flow reactor and *cis*-pinonaldehyde (2 μL) were reacted directly on an ungreased zinc selenide (ZnSe) FTIR disk (25 mm diameter) by adding a small amount of aqueous H_2SO_4 acid catalyst solution (1 wt % H_2SO_4 aqueous solution), and FTIR spectra were measured as a function of reaction time. Organic aerosols were also collected directly on an ungreased ZnSe FTIR disk by impaction from either the 0.5-m^3 Teflon film bags or the 190-m^3 outdoor smog chamber. The scan number for the FTIR was 8, and the resolution was 2 cm^{-1}. The chemicals injected to the flow reactor were measured through a series of two impingers (15 mL of acetonitrile) and detected by a GC/MS. Acid-catalyzed reaction products of *cis*-pinonaldehyde were also applied to the further GC/MS analyses using a Hewlett-Packard 5890 gas chromatograph (30 m, 0.25 mm i.d., J&W DB-5 with 0.25 μm film thickness) interfaced to a 5971 mass selective detector. The GC temperature program for both impinger samples and acid-catalyzed reaction products of *cis*-pinonaldehyde was 70 °C for 1 min, 70−120 °C at 8 °C/min, 120−290 °C at 25 °C/min, and 290 °C for 2 min. The temperature program for the filter and denuder samples from the outdoor smog chamber was 80 °C for 1 min, 80−300 °C at 8 °C/min, and 300 °C for 10 min.

Results and Discussion

The model carbonyl compounds in this study were categorized into three classes: α,β-unsaturated carbonyls, acyclic four-membered ring *exo*-carbonyls, and α-dicarbonyls. All of these three classes of carbonyls are often identified from photooxidation reactions of either biogenic or aromatic VOCs. Many of the aromatic photooxidation products include ring-retaining and ring-opening α,β-unsaturated carbonyls (*19*, *20*). Major carbonyls from α-pinene photooxidation products include acyclic four-membered ring-*exo*-carbonyl structures, such as pinonaldehyde and 10-hydroxypinonaldehyde (*7*, *11*−*17*). Glyoxal and similar α-dicarbonyls (e.g., methylglyoxal and 3-hydroxy-2-oxo-propanal) are products of atmospheric oxidation of aromatics (*20*) or biogenics such as isoprene (*39*). Our previous observations suggest that these carbonyl species can be further transformed via heterogeneous reactions between gas phase and atmospheric particulate matter (*1*, *25*, *30*). The effect is a potential increase in SOA mass because the new aerosol reaction products, which are different from their original parent carbonyls, have relatively low vapor pressures (*13*, *20*).

Class I: Acyclic α,β-Unsaturated Carbonyls. *Aerosol Growth Yields.* The organic aerosol growth yields (*Y*) of different carbonyls by acid-catalyzed heterogeneous reactions are shown in Table 1. The averaged *Y* values for port 7B and 7T (Figure 1) are shown in Figure 2 in the presence and absence of an acid catalyst. The aerosol growth yields (*Y*) are defined here as

$$Y = (\mathrm{Vol}_{\mathrm{OA}} - \mathrm{Vol}_{\mathrm{Seed}})/({}^{i}K_{\mathrm{p}}\mathrm{Vol}_{\mathrm{Seed}}\,{}^{i}C_{\mathrm{g}}) \qquad (1)$$

where $\mathrm{Vol}_{\mathrm{OA}}$ and $\mathrm{Vol}_{\mathrm{Seed}}$ are the volume of the total organic aerosol and the seed aerosol (μL m^{-3}), ${}^{i}C_{\mathrm{g}}$ is the concentration (mg/m^3) of a gas-phase organic (*i*) injected to the flow reactor, and ${}^{i}K_{\mathrm{p}}$ is an absorptive equilibrium−partitioning coefficient (*31*, *40*). It was assumed that the density of organic aerosol is the same as the seed aerosol. The unitless aerosol yield (*Y*) represents the ratio of the experimental organic mass increase to theoretically available particle-phase organic mass in equilibrium partitioning. The ${}^{i}K_{\mathrm{p}}$ in eq 1 is given by

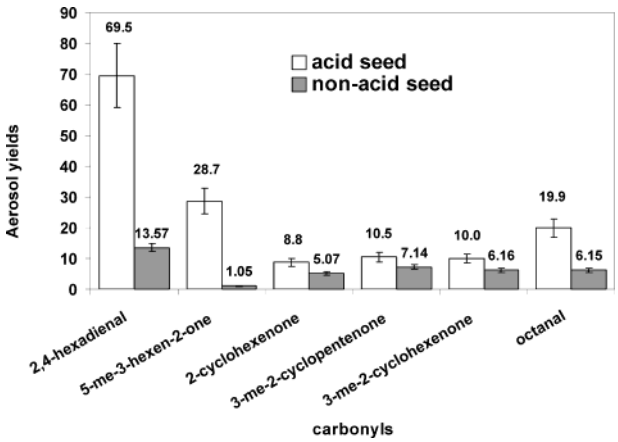

FIGURE 2. Organic aerosol yields of different carbonyls in the presence/absence of an acid aerosol seed catalyst. The aerosol yields were calculated using eq 1. The error bars, which were calculated from the SMPS aerosol population data, were determined at a 0.95 confidence level. On average, the error bars show ±14.9% of a mean.

$$ {}^{i}K_{\mathrm{p}} = \frac{7.501RTf_{\mathrm{om}}}{10^{6}\,\mathrm{MW}_{\mathrm{om}}\,{}^{i}\gamma_{\mathrm{om}}^{\infty}\,{}^{i}p_{\mathrm{L}}^{\circ}}\ (\mathrm{m}^3/\mathrm{mg}) \qquad (2)$$

where *R* is the gas constant (8.314 J K^{-1} mol^{-1}), $\mathrm{MW}_{\mathrm{om}}$ is the average molecular weight (g/mol) of the given organic matter (om), f_{om} is the mass fraction of the absorptive liquid-like material, *T* is the ambient temperature (K), ${}^{i}p_{\mathrm{L}}^{\circ}$ is the vapor pressure (mmHg) of a pure compound (*i*), and ${}^{i}\gamma_{\mathrm{om}}^{\infty}$ is the activity coefficient of *i* at infinite dilution in a given liquid-like medium. The ${}^{i}p_{\mathrm{L}}^{\circ}$ of different carbonyls can be calculated by previously known methods: the group contribution (*33*−*38*) and Antoine regression (*32*). The ${}^{i}p_{\mathrm{L}}^{\circ}$ values are shown in Table 2 along with ${}^{i}K_{\mathrm{p}}$ at 298 K.

The results for aerosol growth yields in Table 1 and Figure 2 indicate that H_2SO_4 as an acid catalyst accelerates heterogeneous reactions of different carbonyls and leads to significantly higher aerosol yields than in the absence of H_2SO_4. The experimental molar ratio of NH_3/H_2SO_4 in the acidified seed was 0.81, leading to the coexistence of NH_4HSO_4 with H_2SO_4. This composition also implies that small amounts of H_2SO_4 are still available as an acid catalyst in the seed aerosol. Our recent studies also showed that the heterogeneous acid-catalyzed reactions of aldehydes are significantly accelerated as the relative humidity decreases (*30*). Future studies at different humidity conditions are needed along with different NH_3/H_2SO_4 molar ratios to demonstrate the acid-catalyzing capability of heterogeneous reaction of organic compounds.

In particular, Table 1 and Figure 2 also show the strong influence of the functional groups and organic carbonyl chemicophysical properties on aerosol growth via acid-catalyzed heterogeneous reactions. In this acid-catalyzed system, aldehydes (e.g., 2,4-hexadienal and octanal) were much more reactive than ketones (e.g., 2-hyclohexenone, 3-methyl-2-cyclopentenone, and 3-methyl-2-cyclohexenone), which eventually resulted in higher aerosol growth. Specifically, the α,β-unsaturated functionality led to higher aerosol yields compared to aliphatic carbonyls (Table 1 and Figure 2). Possible explanations for the high aerosol yields in the aldehyde system as compared to the ketone system are the higher reactivity of aldehydes and the favorable equilibrium constants for the hydrate form of aldehydes.

The increased aerosol yield from introducing α,β-unsaturated functionality to carbonyls is due to the proto-

SCHEME 1. Possible Acid-Catalyzed Reactions of an α,β-Unsaturated Aldehyde in the Particle Phase

Protonation

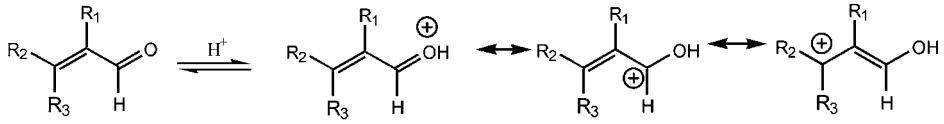

Hydration

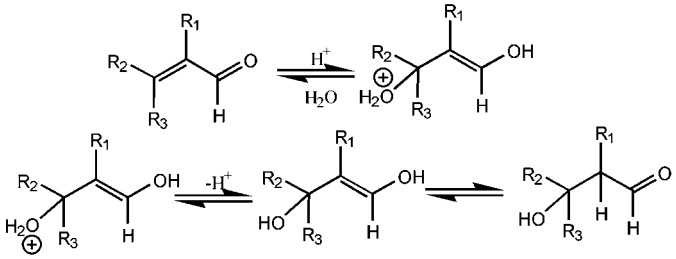

Addition of Alcohol

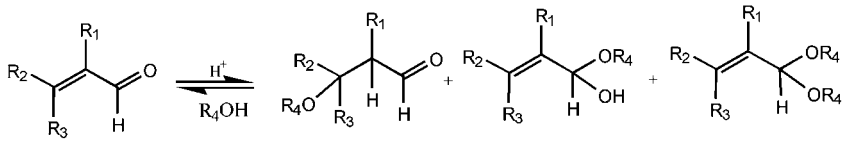

Polymerization

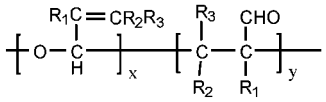

1,2- and 3,4-reaction of conjugated aldehydes

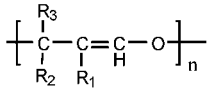

1,4-reaction of conjugated aldehydes

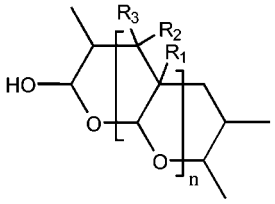

cyclization of conjugated aldehydes

R1, R2, and R3: H or alkyls

nation ability on the oxygen of the different carbonyl species. As shown in Scheme 1, protonation on the oxygen of α,β-unsaturated carbonyls leads to an allylic carbocation, which resonates with a β-position carbocation. Conjugation with an internal olefinic bond increases the basicity of the carbonyl due to the stability of the protonated carbonyl (*41*). Table 2 also shows pK_{BH+} of the carbonyls used in this study. The pK_{BH+} values of α,β-unsaturated carbonyls vary according to either the length of the conjugation or the substituted groups on α,β-double bonds. It is known that the linear dienal/dienone system is a stronger base than the enal/enone analogue by approximately 1.20 pK_{BH+} unit. Substituents, R_2 and R_3, on carbonyl double bonds (Scheme 1) impact pK_{BH+} values because they can influence the stability of the β-position carbocation (*42*). For example, the pK_{BH+} of 3-butene-2-one is −4.8, and the pK_{BH+} of the carbonyl (3-penten-2-one) with a methyl group on the β-position is −3.8. By introducing two methyl groups on the β-position, the pK_{BH+} of 4-methyl-3-penten-2-one is −2.9. This also corresponds to the extent of needed acidity from acid catalysts on heterogeneous reactions. By introducing a methyl group on the β-position of 2-cyclohexenone, the pK_{BH+} drops by about 0.8 units (*41*). Further detail studies for substituent effects on organic aerosol yields and the kinetic mechanisms related to a rate-determining step in acid-catalyzed reactions are needed.

To confirm the organic aerosol formation in a reduced organic concentration and a longer time scale (minutes) than in the flow reactor (seconds), the organic aerosols were also generated in the 0.5-m^3 Teflon film bag in the presence of acid-catalyzed seed aerosols. The percent organic aerosol yields for the Teflon film bag experiments are calculated by the aerosol volume increases normalized by the volume of the seed aerosol and are reported in Table 3 and Figure 3. In general, the results from a Teflon film bag corroborate with observations in the flow reactor. Aldehydes lead significantly higher aerosol yields than ketones. The linear dienal such as 2,4-hexadienal resulted in higher organic yield than a dienal (2-hexenal).

High Molecular Weight Polymeric Structures in Organic Aerosols. Under our experimental conditions, cationic polymerization can be initiated by a protonation from inorganic

TABLE 3. Organic Aerosol Formation in the 0.5-m³ Teflon Film Bag with an Acid Catalyst

expt date (mm/dd/yy)[a]	chemicals	seed (nm^3/cm^3)	aerosol (nm^3/cm^3)	gas concn ($\mu L/m^3$)	% aerosol yield[b]
02/18/03	2,4-hexadienal	1.33E+09	1.19E+11	15.7	0.750
02/18/03	5-methyl-3-hexen-2-one	1.55E+09	1.04E+10	15.8	0.056
02/19/03	2-cyclohexenone	1.61E+09	5.62E+09	18.2	0.022
02/18/03	3-methyl-2-cyclopentenone	1.37E+09	5.01E+09	15.4	0.024
0218/03	3-methyl-2-cyclohexenone	1.22E+09	8.68E+09	15.0	0.050
02/18/03	octanal	1.67E+09	2.36E+11	15.4	1.526
02/19/03	2-hexenal	1.80E+09	5.38E+10	15.8	0.330
02/19/03	mesityl oxide	1.69E+09	3.33E+09	21.9	0.007

[a] The experimental temperature was 294−296 K, and the % RH was 45−47. [b] The % aerosol yield was calculated by 100 × (aerosol volume − seed volume)/seed volume.

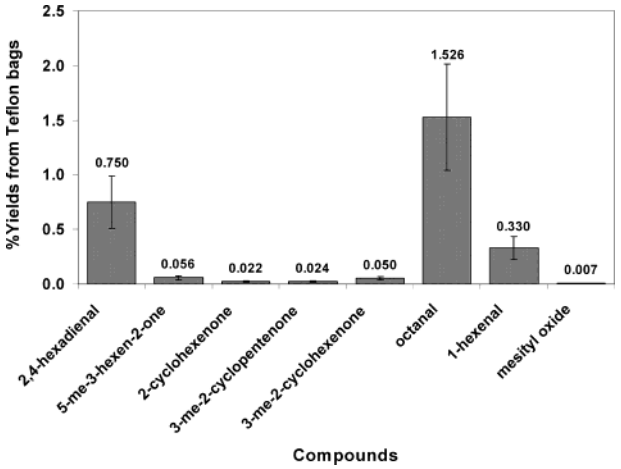

FIGURE 3. Organic aerosol yields obtained from the 0.5-m³ Teflon film bag experiments in the presence of an acid catalyst. The error bars were estimated from the previous 0.5-m³ Teflon bag experimental data for the octanal system under similar experimental conditions (e.g., the volume of seed aerosols, the concentration of the gas-phase octanal, and humidity). On average, the error bars show ±32% about the mean at a 0.95 confidence level.

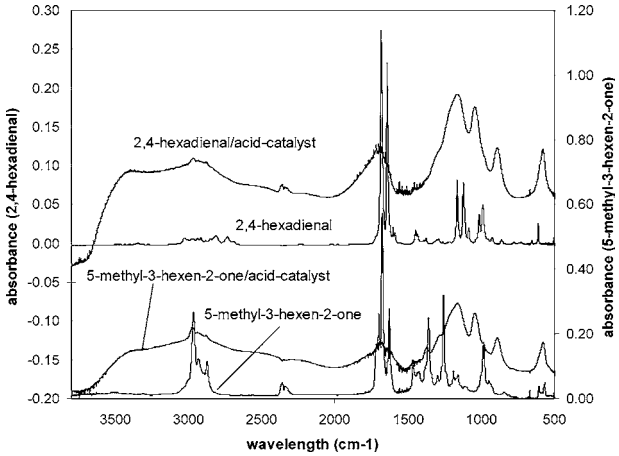

FIGURE 4. FTIR spectra of the acid-catalyzed reaction systems of 2,4-hexadienal and 5-methyl-3-hexen-2-one. The carbonyl (2 μL) was directly reacted on a ZnSe FTIR window by adding small amounts of an aqueous H_2SO_4 catalyst solution (0.1 M, 0.5 μL).

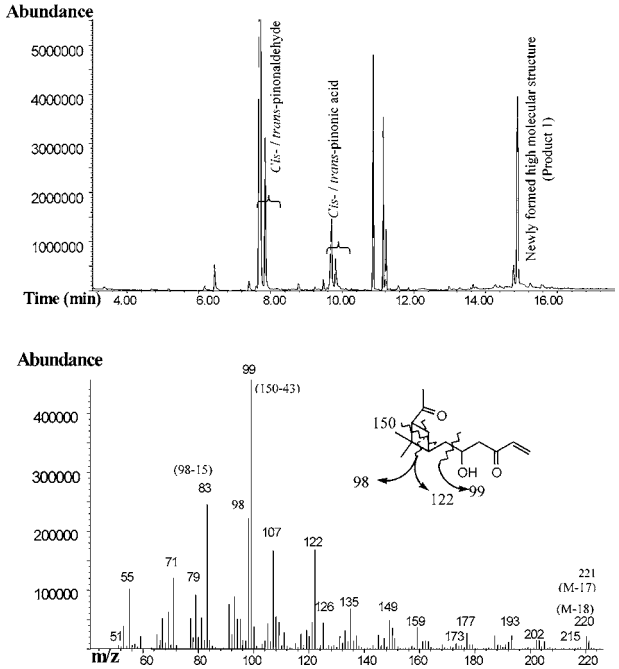

FIGURE 5. GC chromatograms for the *cis*-pinonaldehyde/acid catalyst reaction system (top) and the mass fragmentation of product A at retention time = 14.9 min (bottom).

acids. For example, it has long been known that α,β-unsaturated carbonyls are polymerized in the presence of a strong acid (*43*, *44*) in the bulk phase. Unlike saturated carbonyls, which react on a carbonyl group (1,2-process), the electrophilic acid-catalyzed reactions for α,β-unsaturated carbonyls may react by either a 1,2-, a 3,4-, or a 1,4-process as shown in Scheme 1. In addition, tetrahydropyran rings via cyclization (Scheme 1) and large molecules through either branching or cross-linking can also be formed (*43*, *44*).

FTIR spectroscopy was employed to directly observe functional group transformation as heterogeneous reaction progressed. Unlike the bulk-phase reaction, the reaction at the thin organic layer on the FTIR window (approximate thickness ~ 5 μm) more closely simulates the reaction in the open system such as atmospheric particles. In an open system, the reactants either evaporate into the gas phase or proceed onto products, and water molecules are distributed between gas and particle phases. Figure 4 illustrates the FTIR spectra of the reaction system of 2,4-hexadienal and 5-methyl-3-hexen-3-one in the presence of an acid catalyst. Although not shown here, the other carbonyl systems in the presence of an acid catalyst showed similar FTIR spectra as illustrated in Figure 4. Of interest in the FTIR spectra (Figure 4) is band broadening as the reaction progresses in the condensed phase. Peak broadening in FTIR spectral bands indicates the formation of polymer-like large molecules, which contain a host of diverse structural isomers and conformers.

All acid-catalyzed systems exhibited an O−H stretch at 3100−3600 cm^{-1}, indicating the existence of hydrates of carbonyls. The carbonyl stretch (1650−1730 cm^{-1}) and the alkenyl double bond stretch (1620−1650 cm^{-1}) (*45*) in all systems also dramatically decrease as the reaction processes (*1*, *25*). The FTIR bands at 1170 (C−O−C stretch of polymers),

SCHEME 2. Possible Acid-Catalyzed Reaction Mechanisms of *cis*-Pinonaldehyde in the Particle Phase

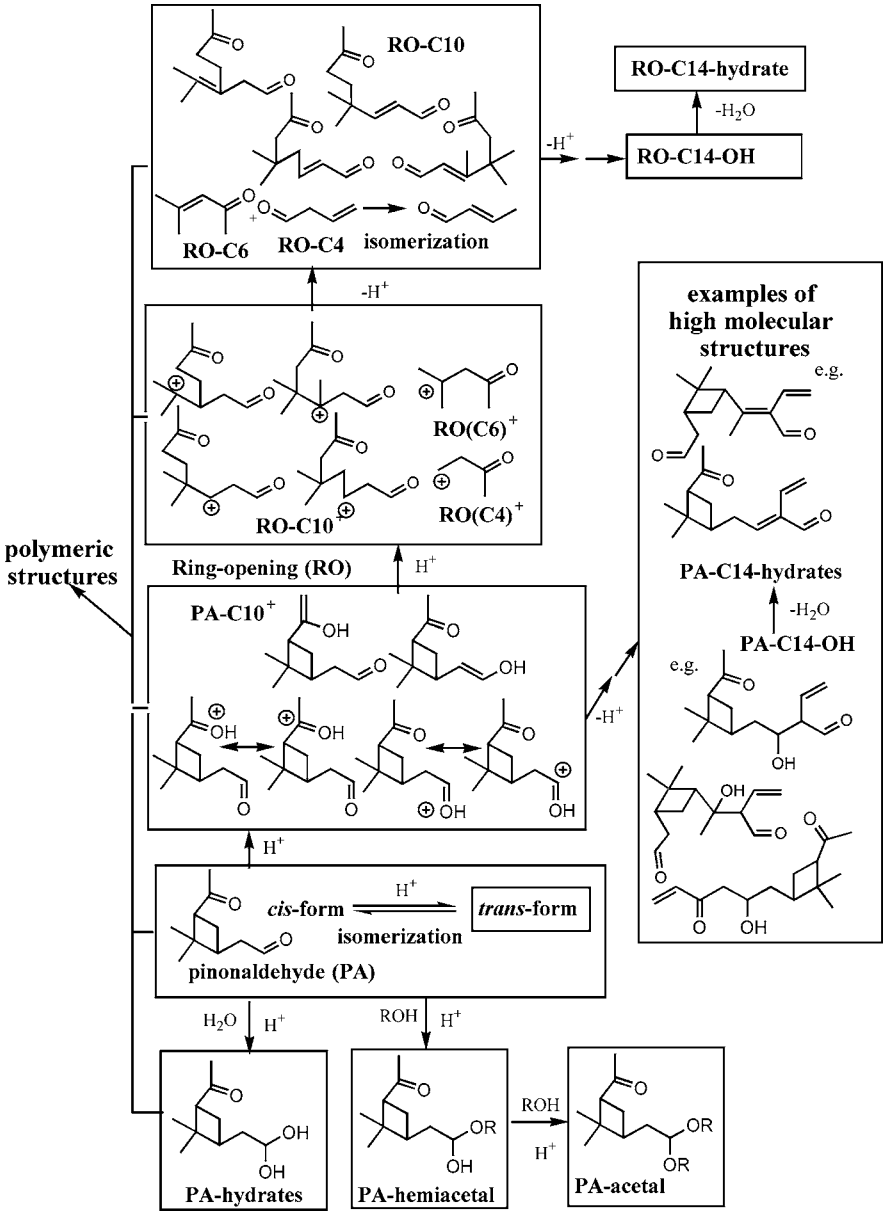

1052 (C−C−O asymmetric stretch of alcohols), 890 (C−C−O symmetric stretch of polymers; symmetric stretch of alcohols), and 578 cm^{-1} (−OH out of plane or C−C−O deformation) also strongly confirmed the functional group transformation of carbonyl species in the presence of an acid catalyst.

Class II: Acyclic Four-Membered Ring *exo*-Carbonyl. *cis*-Pinonaldehyde is a major carbonyl product of α-pinene photooxidation. Figure 5 shows the GC chromatogram of *cis*-pinonaldehyde, which directly reacted in a bulk phase (2 μL) by adding a small amount of aqueous H_2SO_4 acid catalyst solution. The GC chromatogram in Figure 5 clearly illustrates that newly formed products (product A) appeared at retention time of 14.9 min. The mass spectrum of product A is also shown at the bottom of Figure 5 with its tentatively identified molecular structure. Possible acid-catalyzed reaction mechanisms of *cis*-pinonaldehyde are proposed in Scheme 2. The reaction mechanism for product A is also illustrated in Scheme 3. The ring strain in four-membered ring of *cis*-pinonaldehyde leads to ring-opening structures in the presence of an acid catalyst. The primary reactions of *cis*-pinonaldehyde include *cis*−*trans* isomerization, structural isomerization via ring-opening reactions, and ring-cleavage reactions forming α,β-unsaturated carbonyls and carbocations, as show in Scheme 2. The *cis*−*trans* isomerization is a strong feature of the ring-opening process of *exo*-carbonyls such as *cis*-pinonaldehyde. Of interest in acid-catalyzed reactions of *cis*-pinonaldehyde is the creation of higher molecular weight products between different carbonyls and carbocations resulting from hydration, ring-cleavage reactions, aldol condensation, and hemiacetal/acetal formation. Figure 6 illustrates the time series FTIR spectra in the C═O stretch region between 1550 and 1950 cm^{-1} for the *cis*-pinonaldehyde/acid catalyst reaction system. The FTIR spectrum of *cis*-pinonaldehyde shows only two sharp carbonyl stretches at 1722 (aldehyde) and 1705 cm^{-1} (ketone). As the heterogeneous reactions progress, high molecular structures with different C═O and C═C stretches (Scheme 2) are formed, resulting in band broadening in the FTIR spectra as shown in Figure 6.

Class III: α-Dicarbonyls. Recently exploratory experiments in our lab have shown that glyoxal, a simple α-dicarbonyl, showed higher aerosol formation yields in an acid-catalyzed particle-phase environment than aliphatic aldehydes

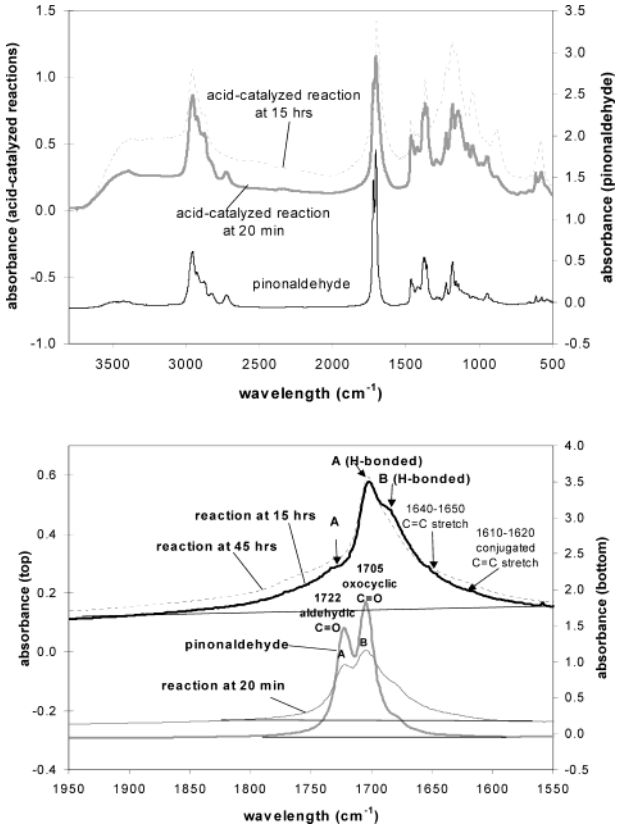

FIGURE 6. (A) FTIR spectra of the *cis*-pinonaldehyde/acid catalyst system as a function of reaction time. *cis*-Pinonaldehyde was directly reacted on a ZnSe FTIR disk by adding small amounts of acid catalyst aqueous solution. (B) FTIR spectra for C═O stretching region of the *cis*-pinonaldehyde/acid catalyst system as a function of reaction time.

SCHEME 3. Reaction Pathway for Product A (MW 238)

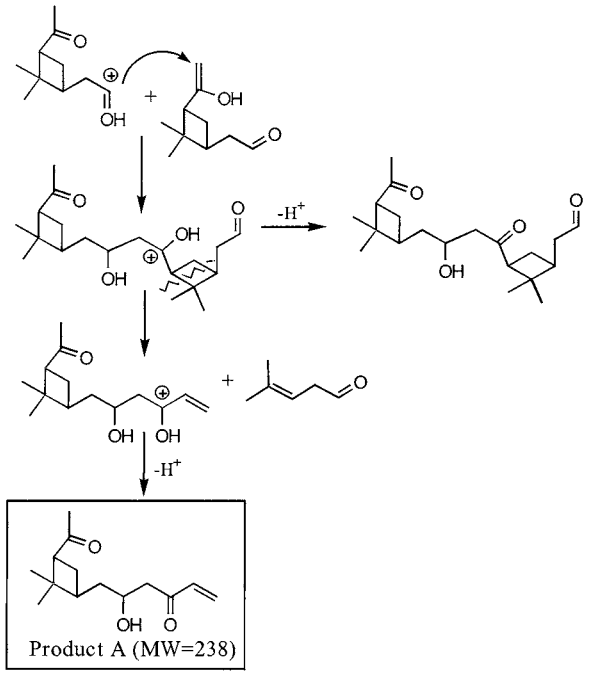

(*25*). It is known that biacetyl and methyl glyoxal are rapidly hydrated and found in fog, clouds, and rain (*46*, *47*). The presence of these compounds in the particle phase may lead to additional pathways for other organic species by particle-phase heterogeneous reactions. In particular, the heterogeneous reactions of glyoxal can be easily explained by hydration and polymerization due to its simplistic structure. Figure 7 shows the FTIR spectra for organic aerosols from the heterogeneous reactions of glyoxal in the presence of an acid catalyst. The carbonyl stretch (1640−1780) in the particle phase almost disappears, indicating that the carbonyl group has transformed. As the aerosols age, the relative intensity of O−H stretch of a hydrogen-bonded alcohol hydroxyl group at 3100−3600 cm^{-1} decreases as compared to FTIR bands at 1180 (C−O−C asymmetric stretch of glyoxal polymers) (*1*, *25*, *48*). A possible explanation for this relative reduction of the O−H stretch is that the hydrate forms of glyoxal are progressively dehydrated and transformed to a polymeric network structure in the organic aerosol phase.

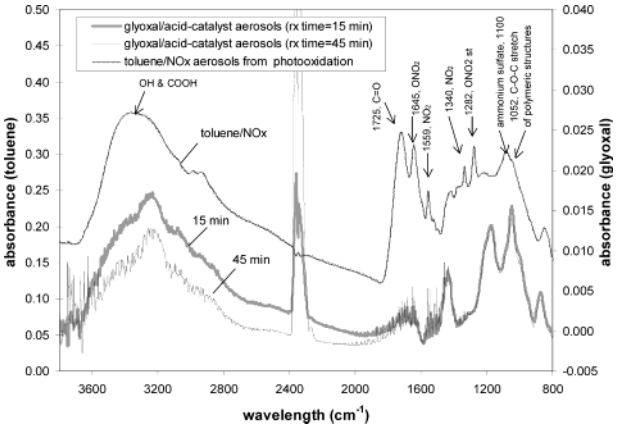

FIGURE 7. FTIR spectra of glyoxal/acid catalyst aerosols and the SOAs formed from the photooxidation of toluene in the presence of NO_x and 1-propene (*20*). The organic aerosols were impacted on the ungreased ZnSe disk. For two different time series, FTIR spectra of aerosol from the glyoxal/$(NH_4)_2SO_4$−H_2SO_4 reaction system (15 and 45 min after aerosol heterogeneous reactions were catalyzed in the 0.5-m^3 Teflon film bag) are shown at the bottom. The toluene photooxidation was conducted in the 190-m^3 outdoor Teflon film chamber (*20*).

Outdoor Chamber Evidence. The ozone reaction with α-pinene to generate SOAs was conducted in the presence of background aerosols, which consist of a mixture of wood soot and diesel soot (*49*). Indigenous sulfuric acid makes up 1.2−5.3% of the mass of the small (mass median diameter ~40 nm) diesel particles at 40% engine load (*28*). In our experimental conditions, it is expected that the SOA formation from the ozone reaction with α-pinene progressed in the presence of the indigenous sulfuric acid on the preexisting particles. Some unsaturated gas-phase constituents of diesel and wood smoke are reacted with ozone and can also produce SOA. However, the major components of SOA are from the ozone reaction with highly reactive α-pinene as evidenced by the rapid changes in the aerosol mass before and after α-pinene injection. The mass fraction of the different aerosol sources was calculated from the TSP, f_{om}, and a tracer for wood smoke (1*H*-phenalen-1-one) in both the east and west chambers. The ratio of wood/diesel/SOA was 0.47:0.19:0.33.

As shown in Figure 8A, the particle-phase products were analyzed to find evidence for acid-catalyzed heterogeneous reactions and high molecular weight product formation. First of all, the most remarkable evidence for acid-catalyzed heterogeneous reactions is the presence of the isomeric structures in cis- and trans-forms for either pinonaldehyde (Figure 8A1) or 10-hydroxypinonaldehyde (Figure 8A2). The ring opening of four-membered *exo*-carbonyl ring structures by acid-catalyzed reaction is necessary in order to obtain the cis- and trans-isomer. The GC peaks (P1−P5), which range from 17 to 24 min in the GC chromatogram (Figure 8A), also

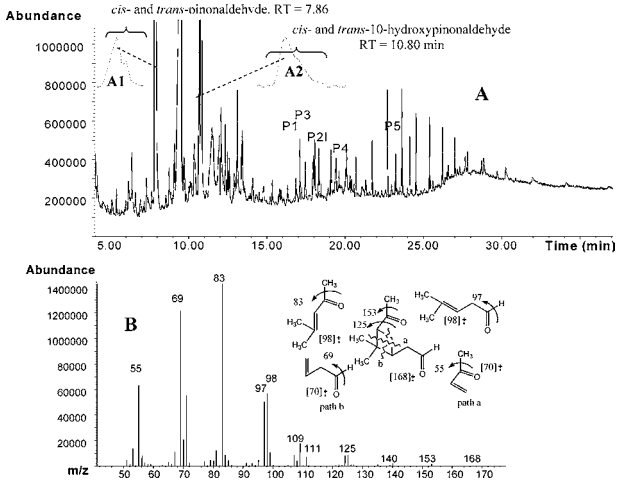

FIGURE 8. (A) GC/MS total ion abundance spectrum for the particle-phase SOA products created from the reaction of α-pinene with ozone in the presence of background aerosols (mixture of 29% of diesel soot and 71% of wood soot). (A1) The expanded GC/MS total ion abundance spectrum for pinonaldehyde. (A2) The expanded GC/MS total ion abundance spectrum for 10-hydroxypinonaldehyde. The injection volume for this GC chromatogram was decreased to obtain improved peak separation. (B) The mass fragmentation of pinonaldehyde and interpretation for each mass fragment.

TABLE 4. Major Carbonyls and High Molecular Structures Tentatively Characterized in the GC/MS Spectrum for Particle-Phase Products from Ozone Reaction of α-Pinene in the Presence of Preexisting Combustion Particulate Matter

product	RT (min)	important fragmentation
pinonaldehyde[a]	7.86	55, 69, 83, 97, 98, 109, 125, 153, 168(MW)
10-hydroxy-pinonaldehyde	10.80	55, 69, 83, 97, 109, 125, 153, 169, 184(MW)
P1	17.10	55, 83, 109, 125, 153
P2	17.78	55, 69, 83, 97
P3	17.92	55, 69, 83, 97, 109, 125, 153
P4	19.66	55, 69, 83, 97, 109, 125, 153
P5	23.20	55, 69, 83, 97, 109, 125, 153, 169

[a] Pinonaldehyde was identified by the standard compound synthesized in our laboratory.

support the presence of the particle-phase high molecular weight structures through the heterogeneous reactions of SOA carbonyls from the α-pinene−ozone reaction. As shown in Table 4, these high molecular structures show similar mass fragmentation patterns, which are characteristic for major carbonyls, such as pinonaldehyde and 10-hydroxypinonaldehyde. Figure 8B also illustrates the mass spectrum of pinonaldehyde along with the interpretation for the mass fragmentation peaks. Conclusively, this result verifies that indigenous sulfuric acid produced from combustion of fossil fuels (e.g., diesel soot and wood soot) can initiate the acid-catalyzed heterogeneous reactions on the particle phase.

Figure 7 illustrates a previously reported FTIR spectrum of SOAs formed from the photooxidation of toluene in the presence of NO_x and 1-propene and then impacted directly on an FTIR disk (*20*). The photooxidation of toluene was conducted in a 190-m^3 outdoor smog Teflon film chamber on May 26, 2000 (*20*). An interesting feature of the FTIR spectrum of the photooxidation products of toluene is the presence of absorption peaks at 852 and 1052 cm^{-1} similar to the glyoxal/acid catalyst aerosols at 873 and 1052 cm^{-1} (Figure 7) and α,β-unsaturated carbonyls/acid catalyst reaction systems (Figure 4). An important note is that the composition of the SOA from the photooxidation of toluene/NO_x/1-propene did not include sulfuric acid in seed aerosol. A possible explanation for the same FTIR peaks that are produced by acid-catalyzed reactions is that dicarbonyls and α,β-unsaturated aldehydes from photooxidation of aromatics (e.g., toluene) are much more reactive than aliphatic aldehydes, heterogeneously react in the presence of mild acids (e.g., HNO_3, α-oxocarboxylic acids, and oxalic acid), and result in polymeric structures or hydrates. It is known that the atmospheric HNO_3 is much more volatile as compared to H_2SO_4 and mostly present in the gas phase. We have also observed that reaction of carbonyls with HNO_3 on FTIR windows. However, future study of potential catalytic effects of HNO_3 on particle-phase heterogeneous reactions should be undertaken due to abundance of HNO_3 in the atmosphere. We believe that these transformations are due to acid-catalyzed heterogeneous reactions, which can be a potential contributor to SOA formation in natural systems.

Acknowledgments

This work was supported by a grant from National Science Foundation (ATM 9708533) and a STAR grant from U.S. EPA (R-82817601-0) to the University of North Carolina at Chapel Hill.

Literature Cited

(1) Jang, M.; Czoschke, N. M.; Lee, S.; Kamens, R. M. *Science* **2002**, *298*, 814−817.
(2) Chan, Y. C.; Simpson, R. W.; Mctainsh, G. H.; Vowles, P. D.; Cohen, D. D.; Bailey, G. M. *Atmos. Environ.* **1999**, *33*, 3237−3250.
(3) Eldering, A.; Cass, G. R. *J. Geophys. Res.* **1996**, *101*, 19343−19369.
(4) Adams, J. M.; Constable, J. V. H.; Guenther, A. B.; Zimmerman, P. *Chemosphere*: *Global Change Sci.* **2001**, *3*, 73−91.
(5) Hansen, J. E.; Sato, M. *Proc. Natl. Acad. Sci.* **2001**, *98*, 14778−14783.
(6) Altshuller, A. P. *Atmos. Environ.* **1983**, *17*, 2131−2165.
(7) Hull, L. A. Terpene Ozonalysis Products. In *Atmospheric Biogenic Hydrocarbons*; Bufalini, J., Arnts, R., Eds.; Ann Arbor Science: Ann Arbon, MI, 1981; Vol. 2, pp 161−186.
(8) Odum, J. R.; Hoffmann, T.; Bowman, F.; Collins, D.; Flagan, R. C.; Seinfeld, J. H. *Environ. Sci. Technol.* **1996**, *30*, 2580−2585.
(9) Odum, J. R.; Jungkamp, T. P. W.; Seinfeld, J. H. *Science* **1997**, *276*, 96−99.
(10) Hoffmann, T.; Odum, J. R.; Bowman, F.; Collins, D.; Klockow, D.; Flagan, R. C.; Seinfeld, J. H. *J. Atmos. Chem.* **1997**, *26*, 189−222.
(11) Jang, M.; Kamens, R. M. *Atmos. Environ.* **1999**, *33*, 459−474.
(12) Kamens, R. M.; Jang, M.; Chien, C. J.; Leach, K. *Environ. Sci. Technol.* **1999**, *33*, 1430−1438.
(13) Kamens, R. M.; Jaoui, M. *Environ. Sci. Technol.* **2001**, *35*, 1394−1405.
(14) Yu, J.; Cocker, D. R.; Griffin, R. J.; Flagan, R. C.; Seinfeld, J. H. *J. Atmos. Chem.* **1999**, *34*, 207−258.
(15) Noziere, B.; Barnes, I.; Becker, K. H. *J. Geophys. Res.* **1999**, *104*, 23645−23656.
(16) Glasius, M.; Lahaniati, M.; Calogirou, A.; Bella, D. D.; Jensen. N. R.; Hjorth. J.; Kotzias, D.; Larsen, B. R. *Environ. Sci. Technol.* **2000**, *34*, 1001−1010.
(17) Jaoui, M.; Kamens, R. M. *J. Geophys. Res.* **2001**, *106*, 12541−12558.
(18) Jeffries, H. E. Photochemical Air Pollution. In *Composition, Chemistry, and Climate of the Atmosphere*; Singh, H. B., Ed.; Van Nostrand Reinhold: New York, 1995; pp 308−348.
(19) Yu, J.; Jeffries, H. E.; Sexton, K. G. *Atmos. Environ.* **1997**, *31*, 2261−2280.
(20) Jang, M.; Kamens, R. M. *Environ. Sci. Technol.* **2001**, *35*, 3626−3639.
(21) Marnett, L. J.; Hurd, H. K.; Hollstein, M. C.; Levin, D. E.; Esterbauer, H.; Ames, B. N. *Mutat. Res.* **1985**, *148*, 25−34.
(22) *Exocyclic DNA Adducts in Mutagenesis and Carcinogenesis*; Singer, B., Bartsch, H., Eds.; International Agency for Research on Cancer: Lyon, France, 1999.
(23) *The Role of Cyclic Nuclein Acid Adduct in Carcinogenesis and Mutagenesis*; Singer, B., Bartsch, H., Eds.; International Agency for Research on Cancer: Lyon, France, 1986.
(24) Schoenfeld, H. A.; Witz, G. *Toxicol. Lett.* **2000**, *116*, 79−88.

(25) Jang, M.; Kamens, R. M. *Environ. Sci. Technol.* **2001**, *35*, 4758−4766.
(26) Reddy, M. S.; Venkataraman, C. *Atmos. Environ.* **2002**, *36*, 677−697.
(27) Reddy, M. S.; Venkataraman, C. *Atmos. Environ.* **2002**, *36*, 699−712.
(28) Tobias, H. J.; Beving, D. E.; Ziemann, P. J.; Sakurai, H.; Zuk, M.; McMurry, P. H.; Zarling, D.; Waytulonis, R.; Kitterlson, D. B. *Environ. Sci. Technol.* **2001**, *36*, 2233−2243.
(29) Cocker, D. R.; Clegg, S. L.; Flagan, R. C.; Seinfeld, J. H. *Atmos. Environ.* **2001**, *35*, 6049−6072.
(30) Jang, M.; Lee, S.; Kamens, R. M. *Atmos. Environ.* **2003**, *37*, 2125−2138.
(31) Jang, M.; Kamens, R. M.; Leach, K.; Strommen, M. R. *Environ. Sci. Technol.* **1997**, *31*, 2805−2811.
(32) Yaws, C. L. *Chemical Properties Handbook*: *Physical, Thermodynamic, Environmental Transport, Safety and Health Related Propertied for Organic and Inorganic Chemicals*; McGraw-Hill: New York, 1999.
(33) Schwarzenbach, R. P.; Gschwend, P. M.; Imboden, D. M. *Environmental Organic Chemistry*; John Wiley & Sons: New York, 1993.
(34) Mackay, D.; Bobra, A.; Chan, D. W.; Shiu, W. Y. *Environ. Sci. Technol.* **1982**, *16*, 645−649.
(35) Zhao, L.; Li, P.; Yalkowsky, S. H. *J. Chem. Inf. Comput. Sci.* **1999**, *39*, 1112−1116.
(36) Zhao, L.; Ni, N.; Yalkowsky, S. H. *Ind. Eng. Chem.* **1999**, *39*, 324−327.
(37) Joback, K. G.; Reid, R. C. *Chem. Eng. Commun.* **1987**, *57*, 233−243.
(38) Stein, S. E.; Brown, R. L. *J. Chem. Inf. Comput. Sci.* **1994**, *34*, 581−587.
(39) Kamens, R. M.; Gery, M. W.; Jeffries, H. E.; Jackson, M.; Cole, E. I. *Int. J. Chem. Kinet.* **1982**, *14*, 955−975.
(40) Pankow, J. F. *Atmos. Environ.* **1994**, *28*, 2275−2283.
(41) *The Chemistry of Enones*: *Part 1*; Patai, S., Rappoport, Z., Eds.; John Wiley & Sons: New York, 1989; pp 317−354.
(42) Jensen, J. L.; Thibeault, A. T. *J. Org. Chim.* **1977**, *42*, 2168−2170.
(43) Ravve, A. *Principles of Polymer Chemistry*, 2nd ed.; Plenum Press: New York, 2000; pp 101−192.
(44) *The Chemistry of Cationic Polymerization*; Plesch, P. H., Ed.; Pergamon Press: New York, 1963; pp 451−476.
(45) *Fourier Transform Infrared Spectrometry*; Elving, P. J., Winefordner, J. D., Eds.; Chemical Analysis Vol. 83; John Wiley & Sons: New York, 1986.
(46) Collett, J. L.; Daube, B. C.; Gunz, D.; Hoffmann, M. R. *Atmos. Environ.* **1990**, *24A*, 1741−1757.
(47) Munger, J. W.; Jacob, D. J.; Daube, B. C.; Horowitz, L. W.; Keene, W. C.; Heikes, B. G. *J. Geophys. Res.* **1995**, *100*, 9325−9333.
(48) Blando, J. D.; Porcja, R. J.; Li, T. H.; Bowman, D.; Lioy, P. J.; Turpin, B. J. *Environ. Sci. Technol.* **1998**, *32*, 604−613.
(49) Chandramouli, B.; Jang, M.; Kamens, R. Gas−Particle Partitioning of Semivolatile Organic Compounds (SOCs) on Mixture of Aerosols in a Smog Chamber. *Environ. Sci. Technol.* **2003**, *37*, 0000−0000.

Received for review October 28, 2002. Revised manuscript received April 15, 2003. Accepted May 23, 2003.

ES021005U